LC-DET-2007-013

Estimation of radiation effects in the front-end electronics of the Electromagnetic Calorimeter using physics events

V. Bartsch[1], M. Postranecky[1], C. Targett-Adams[1], M. Warren[1], M. Wing[1]
[1]University College London

LC-DET-2007-013

November 19, 2007

Abstract

The front-end electronics of the electromagnetic calorimeter of an ILC detector are situated in a radiation environment. Therefore it needs to be checked how the radiation will affect the performance of the electronics. In this paper, physics events and hadron events originating from the machine background have been simulated and radiation effects within the volumes in which the front-end electronics of the electromagnetic calorimeter are placed have been estimated. It is not yet possible to make a final prediction of the effects of the radiation effects because the type of the FPGAs to be used and the final machine parameters of the accelerator will not be decided for several years. Therefore measurements are proposed which can be made in order to estimate the radiation damage for any given FPGA. The radiation damage is estimated by using energy spectra and energy depositions produced for this part of the detector. The method, but not the particle spectrum and the energy depositions, is applicable for electronics in any part of the detector.

1 Radiation Damage

In this section three failure mechanisms due to radiation damage are introduced: single event upsets (SEUs) which change the state of the electronics, increase of the leakage current which can lead to errors of the electronics and cluster displacements which leads to a non-reversible failure of parts of the electronics.

Single event upsets (SEU) can occur in the electronics if a particle (typically a neutron, proton or pion above a certain threshold energy which is about $20\,\mathrm{MeV}$) traverses it and generates enough electron-hole pairs in the active area of the silicon material such that a change in the state of the circuit occurs. Typically these changes can be reset in FPGAs and therefore SEUs do not lead to permanent damage. However in order to reset the FPGAs at a reasonable rate one needs to know the rate at which SEUs occur.

The leakage currents in FPGAs increase due to the creation of deep level traps between the valence and the conduction band of silicon. The leakage current increases linear with the radiation dose. Charge carriers can be easily lifted into the conduction band and therefore the leakage current increases. Depending on the magnitude of the increase, electronics could show errors when the leakage current is similar to the current flowing when the state of the electronics

changes. It is difficult to counteract these errors, but they only occur at high radiation dose of about 3kRad to 300kRad depending on the FPGA type as measured e.g. in [1].

Displacement damage occurs when collisions between incident particles and lattice ions cause the relocation of the recoiled silicon ions. It depends on the fluence. Displacement damage would cause a reduction in carrier lifetime within the conducting channel. This could lead to changes in device timing and distortion of signals leading to a failure of the electronics. This should not be a concern for the low flux expected at the electromagnetic calorimeter of the ILC detector where an annual flux of $10^4 \, / \, cm^2$ is expected at the electromagnetic calorimeter. Studies for the LHC have shown that FPGAs showed no problems at a fluence of $10^{14} \, / \, cm^2$ [2].

2 Geometry

The FPGAs discussed in this note are part of the front-end electronics (FE) of the electromagnetic calorimeter (ECAL) of the ILC detector as proposed in the TESLA TDR [3]. Although newer, slightly different designs are available the effects described in this note should be similar for any of those designs. For the studies, a magnetic field of the TESLA detector solenoid which has the value of $4\,T$ has been simulated. A cross section of the inner parts of the detector is shown in figure 1. The barrel section of the ECAL has an eight-fold geometry, each of which consists of 40 slabs stacked on top of each other. In the direction of the beamline the barrel ECAL consists of 25 slabs. The front end electronics is located at the end of the slabs of the ECAL which are 26 cm wide. In total the ECAL has 8000 slabs each with one FPGA with an area of $1\,cm^2$. The ECAL covers a pseudorapidity η range of $-1.1 < \eta < 1.1$, therefore there is no η dependence of the particles' energy spectrum expected. It is assumed that the FPGAs connected to the end cap of the ECAL are also located at about 1.8 m away from the pipe.
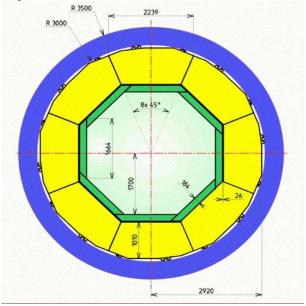

Figure 1: *Cross section and the front end FE of the barrel of the ECAL (inner octagon), hadron calorimeter (middle structure) and solenoid magnet (outer structure).*

process	number of events/h	generated events
t$\bar{\text{t}}$	50-70	110
WW	800-900	183
QCD	$(7\text{-}9)\times10^6$	1987
$\gamma\gamma$ events (machine background)	4.1×10^7	2301
pair production (machine background)	10^{11}	20000

Table 1: *Physics events and machine background which are most relevant for the SEU rate in the FPGAs [3].*

3 Energy spectrum, fluence and radiation dose at the area of the FPGAs

To quantify radiation effects one needs to simulate the energy spectrum of the particles traversing the FPGAs, because these particles cause the radiation damage. In the following, physics events and machine backgrounds will be discussed.

In order to generate the energy spectrum, physics events which occur most often and have a high enough energy in order to traverse the detector and reach the volumes of the ECAL front-end electronics have been chosen. The selection was done with the help of the TESLA TDR [3]. The most probable events according to the TESLA TDR are t$\bar{\text{t}}$ events, WW events and QCD events as shown in table 1. All processes have been generated using PYTHIA [4] and fed into the detector simulation MOKKA [5]. The resulting particle spectra come from the development of showers in the ECAL.

In PYTHIA, events at a centre of mass energy of 800 GeV have been generated. This has been done in order to give a worst case estimate for the radiation damage because the higher energy implies a higher cross section of particles hitting the FPGAs, a higher number of showers and a higher number of particles in each shower. Therefore, the higher the radiation damage. Although the events have been generated at a centre of mass energy of 800 GeV, the production cross section for a centre of mass energy of 500 GeV, which is typically slightly higher than the cross section at 800 GeV, has been chosen according to the TESLA TDR.

For QCD events the beam is composed of electrons, positrons and photons allowing photon interactions to contribute to hadron production. With the option MSTP(14) = 30 one automatically obtains a realistic first approximation to all significant contributions to QCD physics to the total cross section independent of the Q^2 range. WW and t$\bar{\text{t}}$ events do not have photon contributions and therefore have been generated defining the beam to be composed only of electrons and positrons. The WW events were generated with a cut $|\eta| < 2$ in order to reduce the memory allocation of the detector simulation which is proportional to the number of particles simulated. Thus backscattered secondaries are not taken into account for WW and t$\bar{\text{t}}$ events. The WW and t$\bar{\text{t}}$ backgrounds are negligible compared to the QCD background due to their small rates as can be seen in table 1.

For the machine background two types of backgrounds have been considered: machine background arising from incoherent pair production and machine background from $\gamma\gamma$ interactions. The incoherent pair production points into the very forward region of the detector. $\gamma\gamma$ interactions create hadrons, in turn creating jets which can point into the barrel region of the

calorimeter. It has been shown that this background is important for the occupancy of the tracking detector [7].

The event rates expected for a TESLA detector at a collision energy of $800\,\text{GeV}$ are summarized in table 1. The energies of the colliding photons and the outgoing electrons and positrons from pair production have been generated with GUINEAPIG [8]. Special care was taken that there were no cuts made at this stage of the simulation. The resulting photon spectra is shown in figure 2. The energies of the photons were the input collision energies in PYHTIA for an effective photon collider. All particles in the final state were further processed within the MOKKA detector simulation, as with the physics processes discussed previously. For the pair production background the electrons and positrons were used directly in the MOKKA simulation. In the MOKKA simulation, about 25 events out of 20000 have particles traversing the ECAL, however there are no events with particles traversing either the barrel part of the ECAL or the region of the FPGAs. Thus the background from the pair production is lower than the background from the $\gamma\gamma$ interactions as shown later in this note. Therefore this background was discarded for further analysis and just the $\gamma\gamma$ machine background was analysed further.
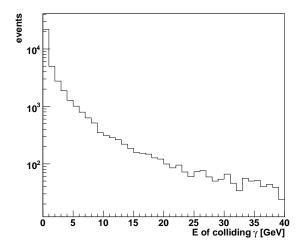

Figure 2: *Energy spectrum of the colliding photons which form the machine background* $\gamma\gamma \rightarrow$ hadrons

After normalising the events to the area covered by the FPGAs the energy spectra of particles in the shower are shown in figure 3. Neutrons, protons and pions create SEUs whereas the other particles do not generate enough electron-hole pairs in silicon in order to generate SEUs. Therefore only these particles need to be considered in the scope of the SEU study.

It is easy to calculate the fluence from the energy spectra using [9]. The $1\,\text{MeV}$ neutron equivalent flux is $2\times10^6\,/\,\text{cm}^2$ per annum. This is about a factor 10^3 smaller than the annual flux of the ILC vertex detector which is dominated by machine background and about a factor of 10^8 smaller than the flux of the inner LHC detectors.

As a third number the radiation dose needs to be calculated. The radiation dose is the electromagnetic energy deposited in a silicon volume and it influences the increase of leakage current. There are two ways to get an estimate for the radiation dose. One way is to calculate the energy deposition from the particle spectra, another way is simulate the energy deposition in the
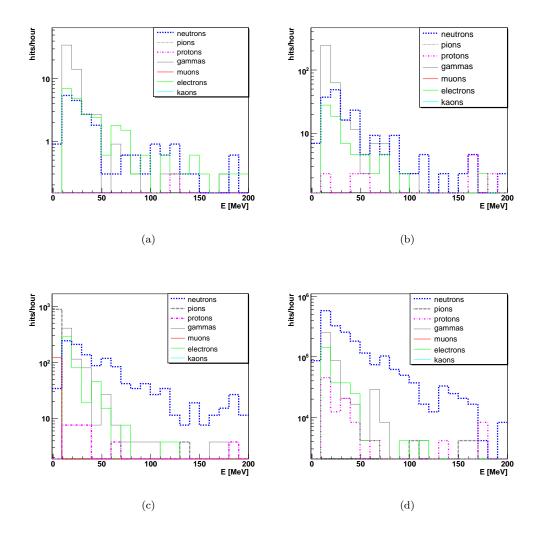
Figure 3: *Energy spectrum at the FPGA for* $t\bar{t}$ *(top left), WW (top right), QCD (bottom left) events and the machine background* $\gamma\gamma \rightarrow$ hadrons *events (bottom right)*

silicon layers of the ECAL and calculate the radiation dose. The energy deposition in 300μm of silicon as a function of each particle is an estimate. It is tabulated in [10]. With this estimate one gets a radiation dose of 7×10^{-4} Rad/year.

The second approach is a worst case scenario. It has been checked that the fourth silicon layer of the ECAL receives most of the energy deposition. With the current MOKKA simulation it is not possible to distinguish between electromagnetic and non-electromagnetic interactions. Only electromagnetic energy depositions contribute to the radiation dose. Therefore we are overestimating the radiation dose. For the simulation of the radiation dose the same events as for the simulation of the energy spectrum have been used. From this simulation the radiation dose is estimated to be 0.13 Rad/year. The two estimates differ by about a factor of 200, but since the numbers are quite small and the estimates are crude, we leave the numbers as it is.

	radiation dose above which errors occurs
Virtex XQVR300 [16]	100kRad
XC4036XL [1]	60kRad
XC4036XL [1]	42kRad

Table 2: *radiation dose above which selected FPGAs show errors.*

4 Estimate of the effects of radiation damage on current FPGAs

Table 2 shows for three FPGAs the radiation dose at which the FPGAs start creating errors. These radiation dose are a factor $>10^5$ higher than the radiation dose we expect per year at the point of the FPGAs at the ILC. This means that we do not expect any problems with this kind of radiation dose.

Tests checking that FPGAs do not fail due to the fluence have been performed for the ATLAS detector at the LHC [2] and it has been confirmed that the current FPGAs do not get affected by this type of damage. We expect a much lower flux at the ILC and therefore propose that this measurement should be done for a given FPGA, however we do not expect a failure of the FPGAs.
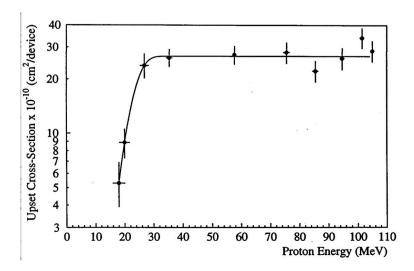

Figure 4: *SEU cross section versus proton energy for the Xilinx XC4036XLA FPGA as measured in [11]*

In order to estimate the SEU rate, it is necessary to measure the SEU rate of FPGAs irradiated with protons, neutrons and pions. Protons, neutrons and pions produce SEUs with the same probability if they traverse above an energy of 20 MeV [11], [12]. Below this energy the protons and pions undergo the Coulomb repulsion between the atomic nucleus and the proton or pion whereas the neutron does not carry a charge and therefore does not interact electromagnetically with the atomic nucleus. This means that neutrons below 20 MeV have a higher probability to cause SEUs than protons and pions. The cross section approximates a step function as shown in figure 4 [11]; below a threshold energy, not enough electron-hole pairs are created to change the state of the circuit, whereas above that energy enough energy is created. Due to geometrical uncertainties like the injection of the particle at an angle, the cross section is not exactly a step function.

type of FPGA	year of publication	citation	$E_{threshold}$ in MeV	σ_{SEU}	SEUs in the ECAL per h
Virtex II X-2V100 and Virtex II X-2V6000	2004	[13]	5	8×10^{-9}	0.55
Altera Stratix	2004	[14]	10	10^{-7}	4.20
Xilinx XC4036XLA	2003	[11]	20	3×10^{-9}	0.09
Virtex XQVR300	2003	[16]	10	2×10^{-8}	0.84
8046RP	1998	[17]	20	10^{-8}	0.29

Table 3: *SEU cross section and threshold energy for different FPGAs as published, rate of SEU in the ECAL calculated from this.*

In table 3 the threshold energy $E_{threshold}$ versus SEU cross section σ_{SEU} for several FPGAs is listed as found in literature. Some papers give the cross section per bit, whereas some papers present the cross section per device. In order to normalise the results it was assumed that one device has one million bits [11]. Unfortunately only proton data were available. Therefore, in order to do an estimate for this study, for protons, neutrons and pions below 20 MeV, the same cross section was assumed for each. This is definitely a systematic error in this study which can not be quantified. If the threshold value of the FPGA chosen for the calorimeter in the end is below 20 MeV it would be advisable to measure for different traversing particle types.

The SEU rate is dominated by the QCD events and the $\gamma\gamma$ machine background events. For the existing measurements the SEU rate for the FPGAs in the ECAL has been calculated. It varies between 14 minutes and 12 hours depending on which FPGA is used. So we advise that the SEU rate of a selected FPGA should be determined before choosing it for the ECAL. However there does not seem to be a dependence of the SEU rate on the production year of the FPGA. Because the size of the circuits within the FPGA will continue to decrease it seems certain the threshold energy of a SEU will decrease. This means that in future it will become more important to measure the SEU cross section σ_{SEU} for protons, neutrons and pions.

5 Occupancy

With the same simulated data we were able to estimate the occupancy of the electromagnetic calorimeter. The occupancy is defined as the number of cells hits within a bunch train divided by the total number of electromagnetic calorimeter cells, 31×10^6. The occupancy is important for the data acquisition system of the electromagnetic calorimeter. Therefore an estimate is given here. In order to get to the number of cell hits per bunch crossing the $t\bar{t}$, WW, QCD events and the machine background events have been combined taking into account the cross section of table 1. In order to get a realistic distribution, the cross section of each physics process has been Gaussian distributed. As can be seen in figure 5 the mean number of hits is about 66000, the highest number of hits about 72000. Taking the highest number of hits the occupancy is 2×10^{-3}. Contributions from noise will increase the occupancy. These studies are beyond the scope of this note.

6 Suggested measurements

In order to measure the leakage current dependency on the radiation dose the current needs to be monitored during the radiation times. A setup is described in detail in [1]. It is generally accepted that the leakage current will decrease if an annealing time is allowed because during
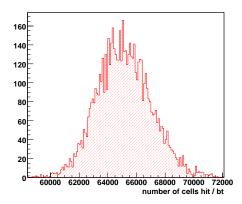
Figure 5: *Number of cells in the ECAL hit per bunch crossing per bunch train.*

that time defects created by the radiation are able to move and either disappear or form more stable defects. Therefore to be on the safe side it is best to do the measurement without allowing any annealing time.

In order to check that a given FPGA does not fail due to cluster displacement one needs to do radiation tests in a neutron testbeam. These tests can be done by applying voltage to the FPGA during irradiation and checking that the FPGAs do not fail. The needed measurements are described in detail in [2].

To test for SEUs (and related problems) errors need to be identified in a functioning FPGA. As FPGAs comprise configuration memory, user memory blocks, registers and combinatorial (non-clocked) resources, as well as task-specific subsystems such as giga-bit serial transceivers, Ethernet hardware and micro-processors, a multi-faceted testing procedure is required.

In most cases less than 10% of the configurable resources inside the FPGA are utilised by user logic [15] due to routing and packing overheads, design element proportions and safety margin. To most efficiently test for SEUs, the firmware needs to exercise as much of the FPGA as possible. Testing a device in a beam is made easier if supporting electronics are not affected by their proximity to the test environment, and should thus be placed physically as far away as possible. By coding the test, error and logging logic into the device-under-test, auxiliary logic can be kept to a minimum, with maximum flexibility. As error checking and logging logic can also be subject to an SEU, duplication is required and the multiple result outputs need to be compared. Figure 6 shows a schematic of a combined combinatorial and register SEU detection module.

Shift registers are used to test a large number of flip-flops, without the possibility of being optimised out of the configuration by the compiler/fitter software. Configuring these as a linear feedback shift register (LFSR) allows a non repeating sequence of (2^{N-1}) states (where N is the length of the shift register in bits). As the sequence from an LFSR is predictable, a pair of identical LFSRs starting in the same state and of the same configuration, clocked by the same clock, will generate exactly the same sequence of binary numbers. If one of these units is affected by an SEU it will no longer match its partner, and an error easily observed. By combining LFSRs with multipliers, large amounts of combinatorial logic can be exercised. Two identical LFSRs, with differing initial states, generate two series of pseudo-random numbers, which are fed into a multiplier. By duplicating the system, discrepancies in the outputs can be
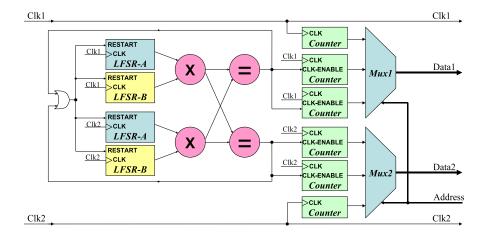
Figure 6: *Schematic showing a firmware module for detecting and logging SEUs in combinatorial and register logic*

easily observed and flagged. To ensure the FPGA is functioning, clock cycles are counted and read out via a data-acquisition system (DAQ).

Monitoring error-flags with a slow DAQ provides a measure of error rate, but during the readout-reset cycle no new errors will be detected. By logging errors to duplicate counters and using the error signal to reset the LFSRs, a portion of the testing can be automated and a more accurate SEU rate measured. A similar method can be used to test RAM resources as LFSRs can be used to generate both addresses and data. Without readout rate constraints, multiplexers, under the control of an external DAQ, can be used to access large numbers of error-counters sequentially. To maximally fill the FPGA, these modules need to be duplicated and/or scaled as needed.

Other FPGA resources can also be tested using synchronised pairs of pseudo-random number generators, each test customised for the specifics of the hardware. For example, giga-bit transceivers can be connected externally to the FPGA and the recieved data from each compared. Embedded microprocessor tests are hardware dependent and need complex software designed to utilise as much of the specific architecture as possible. These methods are beyond the scope of this paper, suffice it to say that many FPGAs have multiple processors and their outputs can be compared and logged as with the other test modules described here.

In addition to user logic the configuration memory inside the FPGA needs to be confirmed uncorrupted. Some FPGAs provide a means of determining these internally, or the configuration memory needs to be checked externally. This can be done by repeatedly reading it out using a PC hosted programming (JTAG) cable and comparing it with the source. Total dose affects are visible as changes in device power consumption, and can be monitored using a power-supply with remote monitoring capability connected to the DAQ

7   Radiation monitoring

In order to monitor the radiation which is actually occurring in the electronics it would be beneficial to monitor the radiation level during operation of the ILC detector with monitoring

devices in a similar way as it is planned for the LHC detectors [18]. One would need one radiation monitor device for each type of radiation damage: a SRAM with a high SEU rate to monitor the SEU effects, silicon diodes for the fluence measurement and a radiation sensitive MOSFET for the measurement of the radiation dose. The SRAM measurement is self-explanatory. The silicon diodes can be used as radiation monitor devices because the effective doping concentration and therefore the depletion voltage are proportional to the fluence [19]. MOSFETs can be used because the flat band voltage at which the energy bands of silicon at the silicon/silicon-dioxide border region are flat depends on the charge density in the oxide. If a particle traverses the silicon/silicon-dioxide region it will create electron-hole pairs in the silicon-dioxide. The electrons which do not recombine move to the silicon/silicon-dioxide border and form the charge density. In a wide range of radiation dose the charge density in the oxide is proportional to the radiation dose. Therefore MOSFETs are a good radiation monitor for the radiation dose. In case one wants to use only one device to measure the fluence and the radiation dose one can use a gate controlled diode [20] which consists of a diode and several MOS rings.

8   Conclusion

This study estimates effects of the radiation damage on the front-end electronics of the electro-magnetic calorimeter in the TESLA design. For this study detector simulations using PYTHIA and MOKKA have been performed for physics events and machine background events which occur frequently according to the TESLA TDR. In this study WW, QCD, $t\bar{t}$, pair production and $\gamma\gamma \rightarrow$ hadrons events were simulated. The particle spectrum of particles traversing the ECAL front-end electronics were generated. The energy depositions in the each layer of the ECAL were calculated. It was shown that all of these simulations were dominated by the $\gamma\gamma \rightarrow$ hadrons machine background and QCD events.

The radiation dose of the fourth ECAL layer was estimated to be around $0.16\,\mathrm{Rad}$ per year due to physics events and therefore does not cause any problematic increase of the current of today's FPGAs. The estimated flux of $2\times10^6/\mathrm{cm}^2$ per annum is too small to cause enough cluster displacements to affect the operation of today's FPGAs. Therefore this study shows that today's FPGAs are able to handle the radiation damage caused by physics events in the front-end electronics of the ECAL. In order to estimate the SEU rates in the whole ECAL, the particle spectra and cross sections for the SEU upsets of today's FPGAs as found in literature were used. It has been shown that the SEU rate with today's FPGAs lies between $14\,\mathrm{minutes}$ to $12\,\mathrm{hours}$ for all of the FPGAs in the TESLA ECAL. This requires the FPGAs in the ECAL to be reset at a higher rate to mitigate these effects.

The SEU rates need to be checked to confirm the final FPGAs behave as those found in today's literature. The measurements necessary for these checks have been briefly discussed. To measure the SEU rate one needs to measure the SEU cross section versus the energy of the incoming particles (e.g. protons). Making use of pseudo random number generators, duplication and error counters, a robust and flexible SEU detection system can be implemented almost entirely within the device under test.

Finally suggestions about radiation monitoring devices have been made. SRAMs can be used for SEU monitoring, diodes for fluence monitoring, MOSFETs for radiation dose monitoring.

With the help of the simulations the occupancy resulting from physics events of the ECAL barrel could be determined. It is estimated to be 3×10^{-3} per bunch train. Again this simulations only comprise physics events and machine background. It is expected that this number will rise when you consider noise.

References

[1] D. MacQueen, Ph.D. thesis, Edmonton, Alberta, 2000

[2] N. Buchanan, M.Sc. thesis, Edmonton, Alberta, 2003

[3] TESLA Technical Design Report, Part IV, A Detector for TESLA, T. Behnke et al., 2001

[4] PYTHIA, JHEP 0605:026, 2006

[5] MOKKA, project page, http://www-flc.desy.de/ilcsoft/ilcsoftware/Mokka/releases/06-02

[6] M. Owen, private communication

[7] Update on $\gamma\gamma \rightarrow$ hadrons Calculation, T. Barklow,http://www-conf.slac.stanford.edu/ alcpg04/WorkingGroups/BeamDeliveryInteractionRegion/ip_bkgnd_hadrons.pdf

[8] D. Schulte, Study of Electromagnetic and Hadronic Background in the Interaction Region of the TESLA Collider, Dissertation, Hamburg, 1996

[9] A. Vasilescu and G. Lindstroem, Displacement damage in silicon, on-line compilation, http://sesam.desy.de/members/gunnar/Si-dfuncs.html

[10] T. Mouthuy, Atlas Internal Note Indet-No-28, 1993

[11] D. Gingrich et al., Proton Radiation Effects in XC4036XLA Field Programmable Gate Arrays, IEEE Transactions on Nuclear Science, Vol. 50, No.2, 2003

[12] M. Huhtinen and F. Faccio, Computational Method to Estimate Single Event Upset Rates in an Accelerator Environment, NIM A450, p 155-172

[13] G. Swift, Xilinx Single Events Effects, 1st Consortium Report, Virtex-II Static SEU Characterization, 2004

[14] A. Alici et al., Radiation tests of key components of the ALICE TOF TDC Readout Module, Proceedings of the 10th Workshop on Electronics for LHC Experiments and Future Experiments, 2004

[15] A. Lesea, P. Alfke, A Thousand Years Between Single-Event Upset Failures, Online TechX-clusives, http://www.xilinx.com/support/techxclusives/1000-techX35.htm

[16] E. Fuller et al., Radiation Testing Update, SEU Mitigation and Availability Analysis of the Virtex FPGA for Space Reconfigurable Computing, 4th Annual Conference on Military and Aerospace Programmable Devices and Technologies, 2000

[17] P. Layton et al., Radiation Testing Results of Cots Based Space Microcircuits, Radiation Effects Workshop, 1998, IEEE

[18] Radiation Monitoring Working Group, homepage: http://lhc-expt-radmon.web.cern.ch/lhc-expt-radmon/

[19] R. Wunstorf, Dissertation, Hamburg, 1992

[20] C. Becker et al., NIM A444 (2000), 605-613